Virginia Commonwealth University
VCU Scholars Compass

Physics Publications

Dept. of Physics

2014

First-principles studies on graphene-supported transition metal clusters

Sanjubala Sahoo
Virginia Commonwealth University, ssahoo2@vcu.edu

Markus E. Gruner
University of Duisburg-Essen

Shiv N. Khanna
Virginia Commonwealth University, snkhanna@vcu.edu

Peter Entel
University of Duisburg-Essen

Follow this and additional works at: http://scholarscompass.vcu.edu/phys_pubs

Part of the Physics Commons

Downloaded from

http://scholarscompass.vcu.edu/phys_pubs/103

First-principles studies on graphene-supported transition metal clusters

Sanjubala Sahoo,[1,a)] Markus E. Gruner,[2] Shiv N. Khanna,[1] and Peter Entel[2]
[1]*Department of Physics, Virginia Commonwealth University, Richmond, Virginia 23284, USA*
[2]*Faculty of Physics and Center for Nanointegration (CENIDE), University of Duisburg-Essen, 47048 Duisburg, Germany*

Theoretical studies on the structure, stability, and magnetic properties of icosahedral TM_{13} (TM = Fe, Co, Ni) clusters, deposited on pristine (defect free) and defective graphene sheet as well as graphene flakes, have been carried out within a gradient corrected density functional framework. The defects considered in our study include a carbon vacancy for the graphene sheet and a five-membered and a seven-membered ring structures for graphene flakes (finite graphene chunks). It is observed that the presence of defect in the substrate has a profound influence on the electronic structure and magnetic properties of graphene-transition metal complexes, thereby increasing the binding strength of the TM cluster on to the graphene substrate. Among TM_{13} clusters, Co_{13} is absorbed relatively more strongly on pristine and defective graphene as compared to Fe_{13} and Ni_{13} clusters. The adsorbed clusters show reduced magnetic moment compared to the free clusters. © *2014 AIP Publishing LLC.* [http://dx.doi.org/10.1063/1.4893328]

I. INTRODUCTION

Graphene is a promising substrate material due to the inertness.[1–3] Its unique electronic structure,[4,5] such as a point-like Fermi surface and linear dispersion of bands near the Fermi level, renders it as a unique material for studying ballistic transport and quantum Hall effect.[6] It can act as a versatile substrate material for nano electronics.[7] It is an attractive material for efficient extraction of light over a wide range of wavelengths enabling for optoelectronic applications.[8] The photoconductivity of graphene is altered by the adsorption of atmospheric gases.[9] This property can be used to develop gas sensors. Apart from these fascinating properties, deposited transition metal clusters on graphene show high catalytic activity.[10–14] Several experimental studies also exist for the chemical activities of Ni,[15] Co,[16] Pt,[17–21] Pd,[22] and Rh[23] clusters on different carbon supports.

Although several studies exist for the magnetic properties of graphene-supported clusters of $4d$ or $5d$ elements such as Pd or Pt, such studies are still quite limited for clusters of ferromagnetic $3d$ elements such as Fe, Co, and Ni. In particular, there are few studies on magneto-crystalline anisotropy that is critical for magnetic storage devices.[24,25] It has been shown that Co dimers adsorbed on graphene show a large magnetic anisotropy.[24] In spite of the fact that many theoretical studies based on density functional theory (DFT) exist for graphene supported Fe, Co, and Ni adatoms and dimers,[26–29] studies for still larger clusters are limited.[30,31] For example, Johll *et al.*[30] and Longo *et al.*[32] have studied the structural, magnetic, and electronic properties of the graphene supported Fe, Co, and Ni clusters only up to 4 atoms. In this work, we deal with still larger clusters consisting of 13 atoms supported on graphene.

It has been reported that presence of carbon vacancies in graphene modifies the physical and chemical properties of graphene significantly.[33–36] In particular, it has been observed that defect sites act as pinning centers and possess high adsorption energies.[37] This property can be used to manipulate materials at atomistic scale; for example, Wang *et al.* have used defect sites of graphene for controlled growth of Fe, Co, and Ni nano particles[38] in their experiments. In fact, due to the two-dimensional hexagonal structure, graphene shows several kinds of topological defects[39] such as pentagonal defects, i.e., a local five-membered ring structure (*5-m*), heptagonal defects, i.e., a local seven-membered ring structure (*7-m*), or a combination of both, known as the Stone-Wales defect.[40,41] Using tight-binding molecular dynamics simulations Lee *et al.*[42] have studied the diffusion, coalescence, and reconstruction of these defects and find that the coalescence of two single vacancies into a double vacancy and thus Stone-Wales type reconstructions are probabilistic. Their calculations also show that four single vacancies reconstruct into two collective 555-777 defects. In view of all these reports, it is worthwhile to study the influence of vacancy type defects in graphene on the properties of deposited clusters.

In the present study, we have placed the closed geometric shell TM_{13} (TM = Fe, Co, and Ni) clusters on both pristine and defective graphene substrates and performed a detailed investigation of the resulting change in geometry, magnetism, and electronic properties of the clusters as well as the substrate. The paper is organized as follows. In Sec. II, we discuss the theoretical method used for our calculations. The results and discussions are in Sec. III which is divided into three subsections. The qualitative features of free TM_{13} clusters are discussed in Sec. III A. Section III B contains results of TM_{13} clusters adsorbed on pristine and defective graphene sheet with a carbon vacancy. Section III C contains results on TM_{13} clusters adsorbed on pristine, *5-m* and *7-m* type

a)E-mail: ssahoo2@vcu.edu

defective graphene flakes. Finally, in Sec. IV, the results are summarized.

II. COMPUTATIONAL METHODS

Calculations have been performed within the framework of DFT using the generalized gradient approximation (GGA). The Perdew-Burke-Ernzerhof (PBE) exchange-correlation functional[43] is used for the exchange and correlation potential. The calculations are performed using the Vienna *ab initio* simulation package (VASP),[44,45] which uses a plane wave basis. The interactions between the core and valence electrons are treated with the projector augmented wave method.[46] The TM_{13} clusters are adsorbed on pristine graphene sheet which consists of a supercell constructed from 5×3 times the primitive cell of hexagonal graphene and contains 60 C atoms. Periodic boundary condition is applied along two directions of the planar graphene supercell while the direction perpendicular to the graphene is treated with open boundary condition by selecting a large vacuum in order to minimize the image interactions. The geometry optimization is done using the conjugate gradient method. The integration in the Brillouin zone is done through a $2 \times 2 \times 1$ k-points mesh. The self-consistent field calculations are carried out with the energy convergence criterion of 10^{-6} eV. The electronic density of states (DOS) are calculated with Gaussian broadening parameter of 0.05 eV and a k-points mesh of $11 \times 11 \times 1$ for graphene sheet.

Graphene flakes (finite chunks of graphene) can be treated as a zero-dimensional system and hence supercell calculations similar to clusters can be performed. In case of the pristine, *5-m* and *7-m* graphene flakes we used hydrogen-terminated clusters $C_{54}H_{18}$, $C_{45}H_{15}$, and $C_{63}H_{21}$, respectively. A supercell size of $23 \times 23 \times 15$ Å^3 is used for pristine and *5-m* graphene flakes and $26 \times 26 \times 15$ Å^3 supercell size is used for *7-m* graphene flake in order to minimize the interaction between the periodic images. The cluster calculations are done at the Γ-point of the Brillouin zone.

III. RESULTS AND DISCUSSION

A. Properties of TM_{13} clusters

The closed shell clusters with icosahedral geometry are highly symmetric and show enhanced stability compared to other geometries.[47–50] Thus, we have selected these closed-shell TM_{13} clusters for our studies to adsorb on graphene. The structures chosen for the studies have the center-to-shell distances ($d_{Center-shell}$) 2.39 Å, 2.33 Å, and 2.32 Å for Fe_{13}, Co_{13}, and Ni_{13}, respectively, which gives the minimum energy. It has been reported earlier that Fe_{13} has two magnetic states with energy separation of 29 meV.[25,51] The high-spin state has a magnetic moment of 44 μ_B/cluster (ferromagnetic), while the low-spin state has a magnetic moment of 34 μ_B/cluster, where the center Fe atom has magnetic moment antiparallel to that of the twelve neighboring Fe atoms.[52] In contrast to Fe_{13}, only one spin state with ferromagnetic alignment for all sites is found for Co_{13} (31 μ_B) and Ni_{13} (8 μ_B). The high spin state of Fe_{13} with 44 μ_B was found to be more stable

and has been used for the studies of adsorption of Fe_{13} cluster on graphene sheets and graphene flakes as discussed in the following subsections.

B. TM_{13} clusters on graphene sheet

The cluster with icosahedral geometry can be adsorbed on the graphene sheet with three possible orientations, namely, the vertex (top of atom) facing graphene, the bonding edge of surface atoms (bond site) facing graphene, or the triangular facet facing the substrate. Among these configurations, for Fe_{13} and Ni_{13} on graphene, the lowest energy structure has the triangular facet of the cluster facing the graphene, whereas for Co_{13} on graphene an orientation with the edge site of the cluster facing the graphene sheet is found to be energetically most favorable. The optimized geometries for the stable configurations are shown in Fig. 1. A complete relaxation for all atoms of TM_{13} clusters deposited on graphene results in distortion of the icosahedral geometry with a slight appearance of the local distortion on the graphene substrate (approximately 1.4%, i.e., the C–C bond length increases from 1.43 Å to 1.45 Å).

Among three types of TM_{13} clusters considered, the maximum distortion is observed for adsorbed Co_{13}, where the center-shell distance (cluster radius) varies from 2.30 Å to 2.51 Å ($\Delta d_{Center-shell} = 0.21$ Å) as compared to that of the adsorbed Fe_{13} and Ni_{13} on graphene with $\Delta d_{Center-shell}$ values of 0.14 Å and 0.12 Å, respectively. The average center-shell distances for TM_{13} clusters are reported in Table I.

Analysis of the TM–C bonds shows that three facet Fe atoms of the Fe_{13} cluster facing the graphene sheet are bonded to six carbon atoms of a hexagonal ring of the graphene sheet. On the other hand for Co_{13}, four Co atoms facing the graphene sheet have a tendency to form bonds with the C atoms. The orientation of the relaxed Co_{13} is such that one of the four Co atoms is bonded to six C atoms of a hexagonal ring of graphene, with the average Co–C bond length of 2.15 Å. As a result of bonding of Co to several C atoms, the magnetic moment of the Co atom is reduced to 0.82 μ_B, while the average magnetic moment for rest twelve Co atoms amounts to 1.68 μ_B. The average Co–C bond length of Co atom bonded
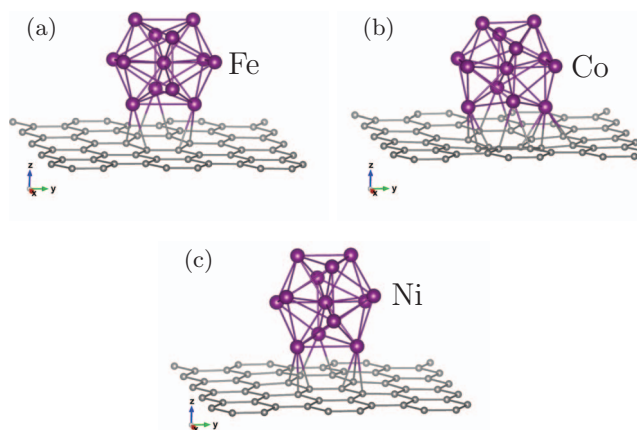

FIG. 1. Optimized structures of Fe_{13} (a), Co_{13} (b), and Ni_{13} (c) clusters on pristine graphene sheet. The dark (purple) and the light (grey) balls represent the TM and C atoms, respectively.

TABLE I. Table showing the adsorption energy E_{Ads} (eV), magnetic moments (μ_B), center to shell distance of the cluster ($d_{Center-shell}$) in Å, and the Bader charges (q^B) of elemental species. M_{Tot}, $\langle M_{TM} \rangle$, and $\langle M_C \rangle$ denote the total magnetic moments, average magnetic moment on TM_{13}, and average magnetic moment on C atoms, respectively. $\langle d_{Center-shell} \rangle$ is the average center to shell distance for TM_{13} clusters. $\langle q^B_C \rangle$ represents the average Bader charge of TM atom in the cluster and on the C atom in the graphene, respectively. The number of electrons treated as valence electrons are 8, 9, 10, and 4 for Fe, Co, Ni, and C, respectively.

| TM | Case | No. of electrons | E_{Ads} | Magnetic moment | | | $\langle d_{Center-shell} \rangle$ | Bader charges (e) | |
				M_{Tot}	$\langle M_{TM} \rangle$	$\langle M_C \rangle$		$\langle q^B_{TM} \rangle$	$\langle q^B_C \rangle$
Fe	Pristine sheet	344	0.882	39	2.789	0.019	2.399	7.919	4.174
	Defect sheet	340	6.837	36	2.578	0.030	2.391	7.884	4.163
	Pristine flake	338	0.667	40	2.837	0.021	2.397	7.943	4.087
	5-*m* flake (concave)	299	2.807	35	2.594	0.010	2.412	7.849	4.112
	7-*m* flake	377	2.502	37	2.681	0.021	2.390	7.898	4.107
Co	Pristine sheet	357	2.144	21	1.618	0.010	2.367	8.914	4.116
	Defect sheet	353	7.998	19	1.490	0.019	2.336	8.886	4.138
	Pristine flake	351	2.021	21	1.614	0.010	2.366	8.916	4.081
	5-*m* flake (concave)	312	4.307	22	1.661	0.010	2.374	8.884	4.109
	7-*m* flake	390	3.716	24	1.709	0.009	2.334	8.914	4.089
Ni	Pristine sheet	370	1.772	8	0.647	0.003	2.348	9.951	4.145
	Defect sheet	366	7.421	6	0.489	0.006	2.357	9.911	4.112
	Pristine flake	364	1.603	8	0.648	0.004	2.349	9.957	4.164
	5-*m* flake (convex)	325	2.973	9	0.696	0.001	2.341	9.955	4.119
	7-*m* flake	403	3.737	7	0.573	0.006	2.354	9.941	4.081

to three C atoms is the smallest with the value of 2.09 Å, while the two Co atoms bonded to two C atoms of graphene have an average bond length of 2.22 Å. On the other hand, the adsorbed Ni cluster on graphene sheet exhibits a similar structural pattern as observed for Fe. Details of the bonding feature can be seen in Fig. 1. The C atoms which are close to the cluster slightly move from their positions in the direction perpendicular to the surface thereby generating a slightly concave (carbon atoms move away from the cluster) or convex (carbon atoms move towards the cluster) topology. The maximum displacement of the carbon atoms is observed for Co adsorbtion, where the carbon atoms move away from the cluster by almost 0.44 Å, similarly for Fe adsorption the carbon atoms move by 0.18 Å, both tending to form concave geometry. On the other hand, Ni adsorption leads to a convex topology, where the carbon atoms move almost 0.23 Å towards the Ni cluster. This observation is also reflected for 5-*m* graphene flake, as is discussed in Sec. III C in the following.

The binding strength between the cluster and graphene is given by the adsorption energy (E_{Ads}), which is defined as

$$E_{Ads} = E_{Tot}^{Cluster} + E_{Tot}^{Graphene} - E_{Tot}^{(Cluster+Graphene)}. \qquad (1)$$

Here, $E_{Tot}^{Cluster}$ is the total energy of free TM cluster, $E_{Tot}^{Graphene}$ is the total energy of (pristine or defective) graphene sheet or graphene flake, and $E_{Tot}^{(Cluster+Graphene)}$ is the total energy of the cluster adsorbed on (pristine or defective) graphene sheet or graphene flake. The E_{Ads} and magnetic moments for the deposited clusters are presented in Table I. Our results show large E_{Ads} for Co_{13} followed by Ni_{13} clusters as compared to that of Fe_{13}. This indicates that Fe_{13} is weakly bound to the pristine graphene. Similar tendency has been also observed for Fe adatom on pristine graphene.[28]

In order to study the adsorption of clusters on defective graphene, we first introduced point defect to the graphene sheet only with a single carbon vacancy in the lattice. The substrate when relaxed show local reconstruction of atoms around the defect for the atoms A, B, and C as shown in Fig. 2(a). The structural distortion has characteristics of the Jahn-Teller (JT) effect,[53] where the system undergoes structural distortions accompanied by the removal of degeneracy of electronic states at the Fermi level. It must be emphasized that we have found two different types of JT distortions with different relaxation settings. In one case a constrained
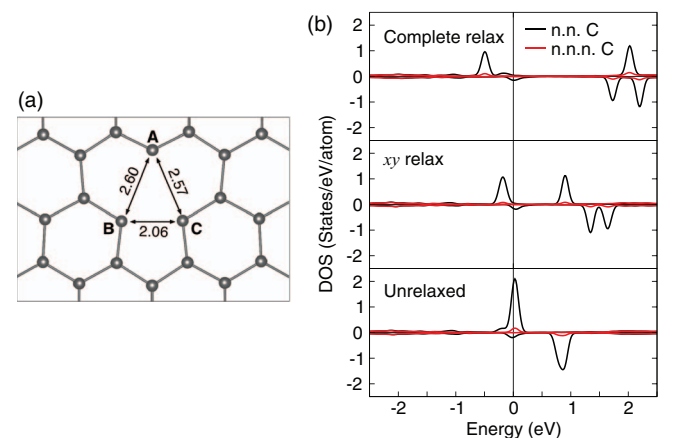

FIG. 2. (a) The local relaxation of graphene sheet with a monovacancy obtained from our calculations, where the grey balls represent the carbon atoms. The relative bond lengths of carbon atoms in close proximity to the vacancy and marked as A, B, and C are shown in Table II. (b) The density of states (DOS) for the unrelaxed (lower panel), relaxation constrained to *xy*-plane (middle panel), and free relaxation (upper panel) of graphene sheet having monovacancy is shown, respectively. The dark solid line (black) indicates the average DOS for carbon atoms nearest neighbor to the vacancy (n.n. C), while the light solid line (red) shows the DOS for the C atoms occupying the next nearest neighbor positions from the vacancy (n.n.n. C). The vertical line represents the Fermi level which is fixed to zero.

TABLE II. Relaxation of graphene with monovacancy constrained to *xy*-plane and free relaxation give two distinct Jahn-Teller distorted structures, which is shown for different total magnetic moment values (M in μ_B). The relaxed structural parameters with respect to Figure 2(a) are tabulated. The largest bond length (d in Å) of the C–C bond around the monovacancy and other two bond lengths referenced to the largest bond length are shown. The energy (ΔE in eV) is shown with respect to the lowest energy obtained for respective type of relaxation.

	Relaxation along *xy* plane			Complete relaxation			
M	ΔE	d_{BC}	d_{AB}/d_{BC}	d_{AC}/d_{BC}	ΔE	d_{AB}	d_{AC}/d_{AB}	d_{BC}/d_{AB}
0.00	0.095	2.653	0.924	0.924	0.116	2.612	0.990	0.800
1.00	0.039	2.639	0.924	0.923	0.030	2.599	0.990	0.786
1.56	0.0	2.641	0.923	0.923	0.0	2.600	0.990	0.791
2.00	0.030	2.649	0.925	0.925	0.050	2.611	0.990	0.896
3.00	0.627	2.621	0.945	0.945	0.732	2.610	0.989	0.803
4.00	1.399	2.563	0.982	0.982	1.685	2.498	0.990	0.800

FIG. 3. Optimized structures of (a) Fe_{13} and Ni_{13}, and (b) Co_{13} clusters adsorbed on graphene sheet with a monovacancy defect. The vertex atom of the icosahedral TM cluster is bonded to the C atoms surrounding the monovacancy. The dark (purple) balls and the light (grey) balls represent the TM and C atoms, respectively.

relaxation with the atomic movement restricted to the *xy* plane (*xy* relax) was done which gave a distorted triangle where the C–C distance d_{BC} is larger than d_{AB} and d_{AC} with $d_{AB} = d_{AC}$. However, we could find another JT distorted structure for defect graphene via relaxation with complete freedom to the atomic movements (complete relaxation). In the latter case d_{BC} was the shortest bond length. The energetics and bond lengths for both relaxation patterns are listed in Table II. The complete relaxed structure is about 3 meV/atom lower in total energy than the *xy* relaxed structure. The complete relaxed structure is in agreement with other DFT studies[31,54–56] and the structure of defect graphene has been observed in experiments under the high resolution transmission electron microscope; see Fig. 3(f) of Ref. 57. The electronic DOS of defective graphene for the two different JT distortions together with the unrelaxed case is shown in Fig. 2(b). The spin polarized DOS for unrelaxed defect graphene shows the states passing through the Fermi energy in both spin channels. After relaxation, the degeneracy is lifted due to the change in crystal field splittings which is a result of deviation from local symmetry due to reconstruction. The crystal field splitting appears more strongly on the nearest neighbor carbon atoms surrounding the vacancy (atoms marked A, B, and C in Fig. 2(a)) for both the relaxed geometry. The splitting is larger in case of the freely relaxed defective graphene.

Figure 2(b) also shows the exchange splitting between the majority and minority DOS due to the appearance of the magnetic moment for the complete relaxed defective graphene. The magnetic moment for the defective graphene sheet is found to be 1.60 μ_B/supercell, which is consistent with previous studies[58] (the unrelaxed structure shows a magnetic moment of 1.18 μ_B/supercell). The magnetic moment is spread nonuniformly on the atomic sites, with the carbon atoms close to the vacancy site having the largest magnetic moment with 0.40 μ_B, while the magnetic moment on C atoms decreases rapidly as the distance from the vacancy site is increased with the carbon atoms reasonably far away from defect site having no magnetic moment. The appearance of magnetic moment in defective graphene is important, especially for studies of TM
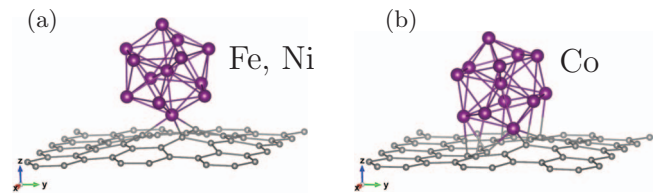
cluster adsorbed on defective graphene as the magnetic moment of defect graphene will interact and influence the magnetic moment of the TM clusters.

The TM_{13} clusters were deposited on to the graphene sheet with monovacancy defect and allowed to relax completely. Figure 3 shows the optimized structures of TM_{13} clusters adsorbed on graphene with monovacancy defect. While Fe_{13} and Ni_{13} are found to be adsorbed in an orientation where one of the vertex atoms of the icosahedral cluster is bonded with the C atoms surrounding the monovacancy site of defective graphene, Co_{13}, on the other hand, relaxes to a tilted orientation owing to its tendency to maximize Co–C bonds. The minimum and maximum bond lengths from the center to the surface atom in Ni_{13} cluster are 2.24 Å and 2.51 Å, respectively, giving a variation ($\Delta d_{Center-shell}$) of 0.27 Å. While, for Fe_{13} and Co_{13} the $\Delta d_{Center-shell}$ are 0.26 Å and 0.22 Å, respectively. This tendency is opposite to that observed for TM_{13} adsorbed on pristine graphene where Co_{13} shows the maximum distortion (previously mentioned). The average center-shell distances for all cases considered are listed in Table I. In addition, the C atoms in the substrate which are close to the clusters show local distortions and are pulled towards the cluster which is most notable for the Co_{13} adsorbed on defective graphene sheet.

The values for the E_{Ads} and magnetic moments for these clusters are shown in Table I. We observe significant enhancement in the E_{Ads} for TM_{13} clusters on defective graphene as compared to that of the clusters adsorbed on pristine graphene because the dangling bonds of the three carbon atoms in the presence of a carbon vacancy are bonded to the TM_{13} cluster, thereby resulting in the stability and lowering the total energy. The E_{Ads} for Co_{13} is found to be more as compared to Fe_{13} and Ni_{13} adsorbed on defective graphene sheet as observed for TM_{13} adsorbed in pristine graphene sheet. This implies that Co_{13} is strongly bound to the defect graphene sheet. Our calculated value of E_{Ads} for Fe_{13} on defective graphene is consistent with previously reported value.[31] We also observe a large charge transfer from cluster to graphene for the case of defective sheet which is 0.12e (Fe_{13}), 0.11e (Co_{13}), and 0.09e (Ni_{13}) as compared to that of the clusters adsorbed on pristine sheet which is 0.08e, 0.09e, and 0.05e for Fe_{13}, Co_{13}, and Ni_{13}, respectively. The amounts of charge on both cluster and graphene are listed in Table I using the Bader charge analysis.[59,60] The average Bader charges on clusters $\langle q_{TM}^B \rangle$ are calculated on the TM atoms close to the graphene substrate forming the nearest neighbor TM–C bonds, similarly,
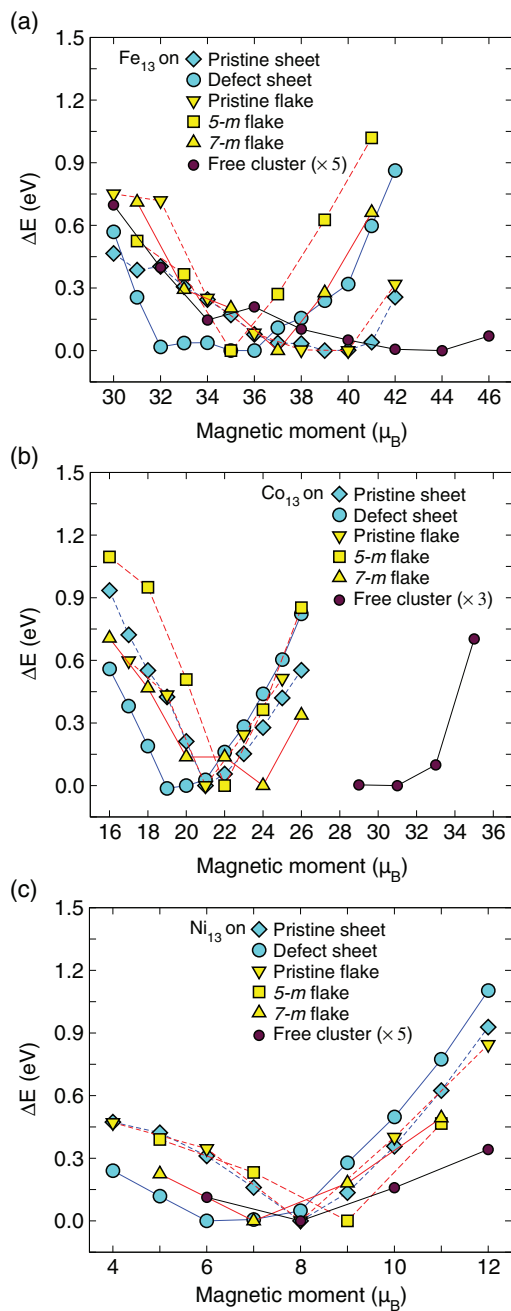
FIG. 4. Variation of the total energy with respect to minimum energy obtained for the adsorbed Fe_{13} (a), Co_{13} (b), and Ni_{13} (c) clusters as a function of fixed spin moment. The symbols diamond, circle, down triangle, square, and up triangle are denoted for pristine graphene sheet, graphene sheet with monovacancy, pristine graphene flake, 5-m graphene flake, and 7-m graphene flake, respectively. The light (yellow) and grey (cyan) fillings of the symbols represent cases for graphene sheet and graphene flakes, respectively. The black line for each case indicates the total energy differences for the free clusters which are multiplied by a factor of five, three, five, respectively, for Fe, Co, and Ni, in order to match the y-axis range.

the average charge on C-atoms $\langle q_C^B \rangle$ are calculated for those C-atoms bonded to the TM atoms.

Figure 4 shows the energy difference (ΔE) obtained with respect to the minimum energy versus the spin moment for various cases of TM_{13} adsorbed on graphene using the fixed spin moment method. The diamond and circle compare the TM_{13} adsorption on pristine and defective graphene sheet,

respectively. The magnetic moments of the adsorbed TM_{13} clusters on pristine and defective graphene are found to be reduced with respect to their corresponding free clusters for Fe and Co. For example, the total magnetic moment for adsorbed Fe_{13} on pristine graphene is found to be 39 μ_B, which is 5 μ_B lower than the magnetic moment of free Fe_{13} cluster with value 44 μ_B/cluster. A larger reduction of magnetic moment is found for Co_{13} (where the total magnetic moment is reduced by 10 μ_B, i.e., from 31 μ_B to 21 μ_B), while for Ni_{13} the magnetic moment remains unchanged. The reduction of magnetic moment on TM_{13} adsorbed on defective graphene is relatively more than the corresponding pristine case, i.e., the total magnetic moment is reduced by 8 μ_B, 12 μ_B, and 2 μ_B for Fe, Co, and Ni clusters, respectively. This is due to the fact that the dangling carbon atoms in the defect graphene are strongly hybridized with the d-states of the cluster atoms, thereby reducing the magnetic moment. The magnetic moment of the vertex atom for Fe_{13} and Ni_{13} adsorbed on defective sheet has lower magnitude. They are estimated to be 0.45 μ_B and 0.05 μ_B in comparison to 2.75 μ_B and 0.53 μ_B for the average magnetic moment of rest twelve atoms for Fe_{13} and Ni_{13}, respectively. In fact, the magnetic moments of Ni atoms vary from 0.44 μ_B to 0.80 μ_B (except the vertex atom facing graphene surface) depending on how far the atoms lie from the graphene surface. In case of Co_{13} cluster deposited on defective graphene, we find that two atoms which are close to the graphene surface have significantly low magnetic moment with values 0.12 μ_B and 1.01 μ_B which are aligned antiparallel to each other. The average magnetic moment per Co atom for other atoms in the cluster amount to 1.66 μ_B. We observe induced magnetic moment on the C atoms in the graphene sheet. The induced magnetic moment has a value of 0.23 μ_B for adsorbed Fe_{13}, 0.12 μ_B for adsorbed Co_{13}, and 0.05 μ_B for adsorbed Ni_{13} on graphene. Similar effects have been previously observed for adatoms adsorbed on graphene.[27] The value of the magnetic moments for TM_{13} adsorbed on pristine and defective graphene are tabulated in Table I.

A recent theoretical study by Gao *et al.*[61] for Ni clusters (up to nine atoms) adsorbed on monovacancy defect graphene has shown that the ground state geometry of Ni cluster is a configuration where one of the Ni atoms lies at the other side of graphene sheet than the rest of the atoms in the cluster. In order to check whether 13-atom icosahedral clusters also prefer such type of distribution of atoms as a low-energy structure, we performed additional calculations where we deliberately moved the vertex atom of the cluster facing the graphene sheet with monovacancy to the other side of the surface. Thus one adatom and a twelve atom cluster lie on two sides of the graphene sheet facing each other through the monovacancy defect. After performing the structural optimization, the total energies are compared with the case of 13-atom icosahedral cluster adsorbed on one side of the defected graphene sheet which have been systematically used in the present study. We find that clusters on one side of the graphene sheet are energetically more favorable than the case where one atom of the cluster lies on the opposite side of the sheet. The energy difference amounts to 84.41 meV/atom, 33.36 meV/atom, and 19.62 meV/atom for Fe, Co, and Ni, respectively. The relaxed structures of TM clusters with one of the TM atoms lying on

the opposite side of graphene surface show that the adatom is bonded to the three C atoms of the substrate surrounding the monovacancy. The relaxation of rest twelve atoms is significant for Ni which undergoes a lateral displacement such that one of the vertex atoms is bonded to the three carbon atoms surrounding the monovacancy. This leads to the formation of one Ni–Ni bond between the Ni atoms placed on the opposite side of the graphene sheet through the vacancy region. This is unlike the Fe and Co clusters, where the twelve atom clusters were observed to have closed geometry. While the total magnetic moment of Co_{13} cluster did not change, the total magnetic moment of Fe_{13} cluster is reduced by 4 μ_B to a value of 32 μ_B, while the total magnetic moment of Ni_{13} cluster is increased by 2 μ_B to give 8 μ_B (compare the total magnetic moment for the cluster adsorbed on one side of defective graphene sheet from Table I).

C. Clusters on 5-*m* and 7-*m* graphene flakes

In addition to clusters supported on graphene sheet, we have studied the adsorption of TM_{13} clusters on graphene flakes. The graphene flakes consist of finite chunks of graphene and are passivated with H at the edge carbon atoms, which we name as *pristine graphene flake*. In order to study the role of defects in the graphene flakes on the adsorption of TM_{13} clusters, we consider the pentagonal and heptagonal structural defects, namely, 5-*m* and 7-*m* graphene flakes. The hydrocarbon clusters with $C_{54}H_{18}$, $C_{45}H_{15}$, and $C_{63}H_{21}$ are considered in our studies for the pristine, 5-*m* and 7-*m* graphene flakes, respectively.

For clusters on pristine graphene flake, the optimized structures of Fe_{13} and Ni_{13} are shown in Fig. 5(a) (owing to the similarity in geometry, they are shown in one figure) and that of the Co_{13} in Fig. 5(b). The structural configurations are similar to that of the respective TM_{13} clusters adsorbed on pristine graphene sheet (refer Fig. 1). Similar to that of the pristine graphene sheet, Co_{13} is adsorbed on pristine graphene flake with an orientation where one of the Co atoms is bonded to six C atoms of a hexagonal ring of the graphene flake. As a result, the magnetic moment of the Co atom is reduced to a value 0.63 μ_B as compared to the average magnetic moment of other twelve Co atoms as 1.69 μ_B/atom. Such drastic reduction of atomic moment of one of the atoms is not observed for Fe_{13} adsorbed on graphene flake, while for Ni_{13}, the atomic magnetic moment varies from 0.35 μ_B to 0.83 μ_B—the farther the Ni atom from the surface of graphene flake, the larger is the magnetic moment. These tendencies are similar to TM_{13} adsorbed on pristine graphene sheet. The E_{Ads} and magnetic moments of these clusters on both 5-*m* and 7-*m* graphene flakes are listed in Table I. It shows that the E_{Ads} for TM_{13} clusters is enhanced for the defect graphene flakes compared to that of the pristine graphene flake. The optimized structures for clusters on graphene flakes (pristine and defective) are shown in Fig. 5. TM_{13} clusters on 5-*m* graphene flake have a large binding strength compared to those of on 7-*m* graphene flake for Fe and Co. Similar trends have been observed from DFT for Pt_{13} and Au_{13} clusters adsorbed on 5-*m* and 7-*m* graphene flakes.[62] However, Ni_{13} shows an opposite behavior where the E_{Ads} of Ni_{13} on 7-*m* graphene flake is en-
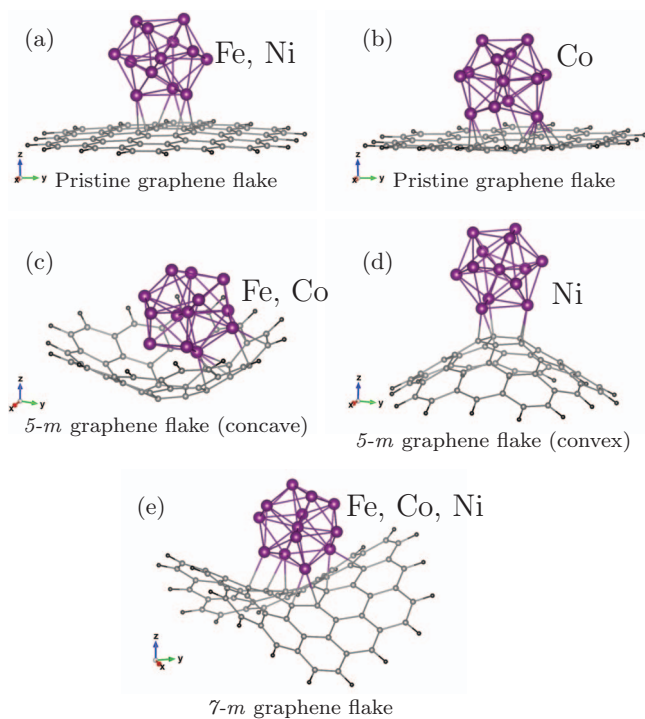

FIG. 5. The optimized structures of (a) Fe_{13}, Ni_{13} and (b) Co_{13} on pristine graphene flake. The low energy structures of Fe_{13} and Co_{13} adsorbed on 5-*m* graphene flake are shown in (c), while the low energy structures of Ni_{13} adsorbed on 5-*m* graphene flake are shown in (d). It must be noted that while Fe_{13} and Co_{13} favor a concave structure as in (c), Ni_{13} favors convex structure when adsorbed on 5-*m* graphene flake. The optimized structures of Fe_{13}, Co_{13}, and Ni_{13} on 7-*m* graphene flake are shown in (e). Owing to the similarity in optimized structures, only one figure is used for representation. The larger dark shaded balls (purple), the light balls (grey), and smaller dark balls (black) represent the TM, C, and the passivating hydrogen atoms, respectively.

hanced relative to the 5-*m* graphene flake. This is attributed to the different structural changes and the bending behavior of the 5-*m* graphene flakes. The adsorption of TM_{13} clusters on 5-*m* graphene flake results in two different bending trends, namely, the concave geometry (where the 5-*m* graphene flake bends towards the cluster allowing for maximum coordination of the carbon atoms) and the convex geometry (where the 5-*m* graphene flake bends away from the cluster). The energetics and magnetic moments for the concave and convex geometries of TM_{13} clusters are listed in Table III. For Fe_{13} and Co_{13}, it is found that the concave geometry is energetically more favorable, whereas for Ni_{13} the convex geometry is more favorable. Moreover, a reduction in the total magnetic moment is observed for Fe_{13} and Co_{13} clusters on 5-*m* graphene flake, whereas for Ni_{13} the moment remains unchanged with respect to the free Ni_{13} cluster. Among the adsorbed clusters on graphene flakes, Fe_{13} and Co_{13} are strongly bound to the 5-*m* graphene flake with the E_{Ads} values of 2.81 eV and 4.31 eV, respectively, while Ni_{13} is strongly bound to 7-*m* graphene flake with binding energy of 3.73 eV. The optimized geometry of TM_{13} on 7-*m* graphene flake is similar, which is shown in Fig. 5(e). Due to the topology of the 7-*m* graphene flake, there is a possibility for the higher coordination of C atoms around the TM atoms. We find that the average nearest neighbor bond length of Fe–C, Co–C, and Ni–C are 2.18 Å, 2.10 Å, and 2.05 Å, respectively.

TABLE III. The total energy differences ($\Delta E = E_{\text{Concave}} - E_{\text{Convex}}$) in eV for the relaxed low energy structures and their corresponding magnetic moments (μ_B) for TM_{13} clusters on concave and convex structures of *5-m* graphene flake as represented in Figs. 5(c) and 5(d), respectively. $\langle d_{\text{Ring}} \rangle$ is the average C–C bondlength (defined as the average over six C atoms in the ring) in the *5-m* graphene flake.

		Concave		Convex	
Cluster	ΔE	$\langle d_{\text{Ring}} \rangle$	M	$\langle d_{\text{Ring}} \rangle$	M
Fe_{13}	−0.435	1.429	35.0	1.455	39.0
Co_{13}	−1.159	1.425	22.0	1.461	24.0
Ni_{13}	0.105	1.425	9.0	1.455	9.0

The plots in Fig. 4 show that the magnetic moment of TM_{13} clusters on defect sheet can be sensitive to the surrounding environment and the external magnetic fields as the energy differences for slight deviation of magnetic moment from the low energy magnetic states are rather low. Fe allows for the change in magnetic moment of about 4 μ_B (32 μ_B/cluster to 36 μ_B/cluster, roughly), similarly, Co allows for 2 μ_B (19 μ_B/cluster to 21 μ_B/cluster, roughly) and Ni allows 2 μ_B (6 μ_B/cluster and 8 μ_B/cluster, roughly). On the other hand, the magnetic moment changes for TM clusters deposited on pristine and defective graphene flakes are associated with large changes in total energies. This suggests that the TM cluster-graphene flake system can be treated as system with giant spins. Large magnetic moment and high magnetic anisotropy are requisite for technological applications. Keeping this in mind, we calculated the magneto-crystalline anisotropy by considering the contribution due to spin-orbit coupling. We have obtained magnetic anisotropy energy of 1.126 meV for Ni_{13} cluster on convex *5-m* graphene flake, which is several orders of magnitude higher than Ni bulk (2.7 μeV/atom). The orbital moments along the easy and hard axes are found to be 0.98 μ_B and 0.96 μ_B, respectively. Bader

charge (q^B) analysis of average atomic charges on the TM atom and on C atom shows that there is a transfer of electronic charges from the TM atoms of cluster to the C atoms of graphene. The results are tabulated in Table I. It is observed that the amounts of charge transfer are slightly increased for Fe and Co clusters adsorbed on *5-m* and *7-m* graphene flakes as compared to Fe and Co clusters adsorbed on pristine graphene flake. An opposite tendency is observed in case of Ni cluster adsorbed on *5-m* and *7-m* graphene flakes as compared to Ni cluster adsorbed to pristine graphene flake where the charge transfer decreases. For all the cases of TM adsorbed on various types of graphene substrates, the E_{Ads} is found to be proportional to the charge transfer from the TM atoms of the cluster to the carbon atoms of graphene. As observed from Table I, we note that although the E_{Ads} varies in the order of E_{Ads} (pristine flake) $< E_{\text{Ads}}$ (*7-m* flake) $< E_{\text{Ads}}$ (*5-m* flake), for Fe and Co clusters, the magnetic moments do not follow similar trend. This is because of the structural orientation of Co_{13}, where the vertex Co atom has very low magnetic moment due to the bonding with six C atoms form a hexagonal ring of pristine graphene flake. Similar structural orientation is also found for Co_{13} adsorbed on pristine graphene sheet, which is already discussed.

In order to analyze the variations in the magnetic moment for Fe_{13}, Co_{13}, and Ni_{13} clusters deposited on the *5-m* graphene flake between the two curvatures and the preference of the convex shape for Ni_{13}, we have plotted the site and the orbital projected DOS for the lowest energy structures for Fe_{13} and Co_{13} (cluster on concave *5-m* graphene flake) in Fig. 6. For Ni_{13}, the corresponding DOS for the concave and convex configurations are plotted in Fig. 7. We first consider the concave geometries for all the clusters. Note that the mixing between the C *p*-states and the TM *d*-states changes with the elemental species of the cluster. The mixing is strongest for Co_{13} and weakest in case of Ni_{13}. In fact, the width of the *d*-states is the lowest for the case of Ni_{13}. A change from
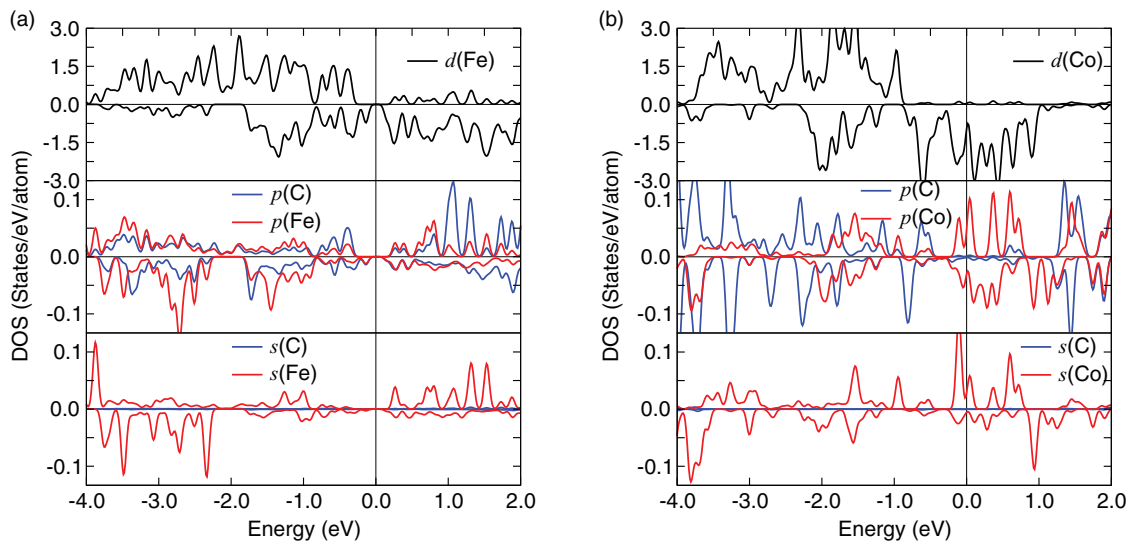

FIG. 6. Site and orbital projected average DOS of elemental species for Fe_{13} (a) and Co_{13} (b) on concave *5-m* graphene flake (as shown in Fig. 5 (c)), respectively. The average *d*-orbital contribution of the TM atoms is shown as black solid line in the upper panels, the dark (blue) and light (red) solid lines show the average *p*-orbital contribution from C and TM atoms in the middle panel, and the dark (blue color) and light (red color) solid lines show the average *s*-orbital contribution from C and TM atoms in the lower panel, respectively. The vertical lines represent the Fermi level which is set to zero.
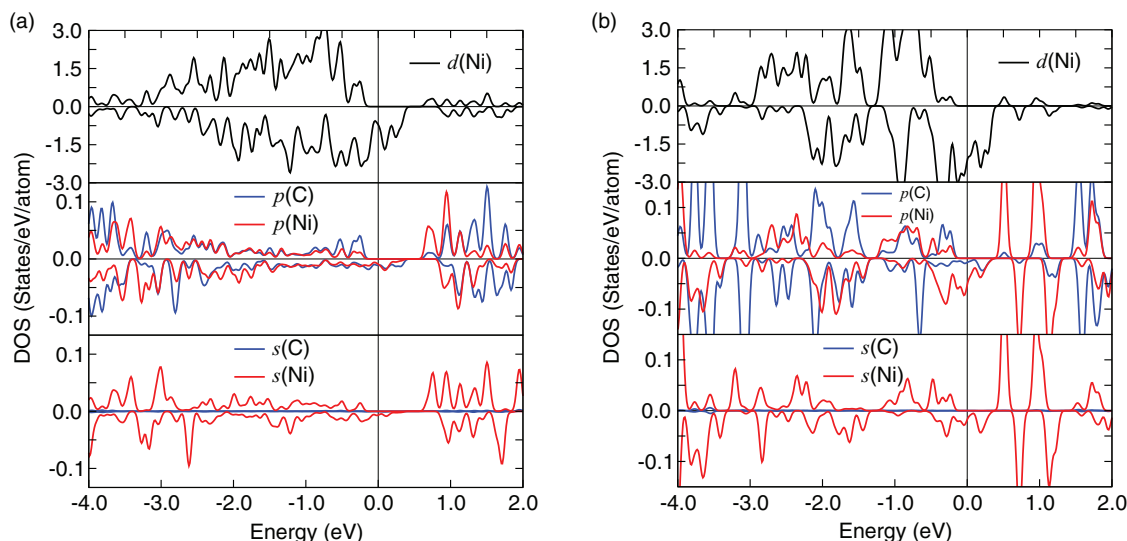
FIG. 7. Site and orbital projected average DOS of elemental species for Ni_{13} on concave (a) and convex (b) *5-m* graphene flake (as shown in Fig. 5 (d)), respectively. The average *d*-orbital contribution of the TM atoms is shown as black solid line in the upper panels, the dark (blue) and light (red) solid lines show the average *p*-orbital contribution from C and TM atoms in the middle panel, and the dark (blue) and light (red) solid lines show the average *s*-orbital contribution from C and TM atoms in the lower panel, respectively. The vertical lines represent the Fermi level which is set to zero.

convex to concave bending is expected to alter the mixing between the carbon *p*-states and the TM *d*-states (carbon *s*-states are deeper in energy). In particular, any change in the mixing with the *d*-states is expected to change the magnetic moment. In view of the large hybridization, the change is expected to be maximum for the case of Co_{13} and lowest for the case of Ni_{13}. Our calculated values indeed confirm this as Co_{13} undergoes a change in moment by 4 μ_B as opposed to 2 μ_B for the case of Fe_{13} and no change in the case of Ni_{13}. Figure 7 also shows that the convex shape allows a slightly better mixing between the C *p*-states and Ni *d*-states than the concave shape. The better mixing is consistent with the change in curvature to convex curvature for the case of Ni_{13}.

IV. SUMMARY

To summarize, we have examined the suitability of pristine graphene, defected graphene, pristine graphene flakes, and defected graphene flakes as support for transition metal clusters. Our investigations have been motivated by the fact that free clusters, while interesting, need to be supported for practical applications. The present investigations bring out three important features. First, the clusters are more strongly bound to the defected sheets and flakes indicating that the defected systems are needed for stabilizing the clusters. Second, the binding to the defected graphene (both sheets and flakes) does not reduce the cluster magnetic moment significantly compared to that of those on pristine sheet. For Fe_{13}, the magnetic moment of the cluster deposited on *5-m* graphene flake is 35 μ_B only slightly reduced from the cluster deposited on pristine sheet, i.e., 39 μ_B. On the other hand, Co_{13} and Ni_{13} undergo an enhancement of the magnetic moment as compared to that of the pristine sheet of values of 21 μ_B/atom and 8 μ_B/atom to 22 μ_B/atom and 9 μ_B/atom, respectively, even though the deposition entails binding with carbon sites. Finally, and surprisingly, the cluster deposition in the case of

Ni_{13} on *5-m* graphene flake leads to a significant enhancement of the magnetic anisotropy by a factor of ~420 times compared to the bulk value of 2.7 μeV/atom. This is particularly surprising since the conventional approach to enhance anisotropy is to deposit clusters on substrates such as Pt marked by high spin-orbit coupling. Here, the enhancement is mediated by carbon that is non magnetic with no significant spin-orbit coupling. One of the quantities of interest is the robustness of the magnetic moments. Figure 4 shows that the magnetic states on the *5-m* graphene flakes are fairly robust as any change in magnetic moment involves a larger change in energy of the system. We hope that the present work will stimulate the experimental studies for clusters on graphene sheets and flakes to investigate the changes in magnetic moments and magnetic anisotropies.

ACKNOWLEDGMENTS

[1] A. Stiles, *Catalyst Supports and Supported Catalysts: Theoretical and Applied Concepts* (Butterworths, 1987).
[2] A. V. Melechko, V. I. Merkulov, T. E. McKnight, M. A. Guillorn, K. L. Klein, D. H. Lowndes, and M. L. Simpson, J. Appl. Phys. **97**, 041301 (2005).
[3] E. Auer, A. Freund, J. Pietsch, and T. Tacke, Appl. Catal. A **173**, 259 (1998).
[4] P. R. Wallace, Phys. Rev. **71**, 622 (1947).
[5] A. H. Castro Neto, F. Guinea, N. M. R. Peres, K. S. Novoselov, and A. K. Geim, Rev. Mod. Phys. **81**, 109 (2009).
[6] A. K. Geim and K. S. Novoselov, Nat. Mater. **6**, 183 (2007).
[7] T. J. Echtermeyer, M. C. Lemme, J. Bolten, M. Baus, M. Ramsteiner, and H. Kurz, Eur. Phys. J. Special Topics **148**, 19 (2007).
[8] K. J. Tielrooij, J. C. W. Song, S. A. Jensen, A. Centeno, A. Pesquera, A. Zurutuza Elorza, M. Bonn, L. S. Levitov, and F. H. L. Koppens, Nat. Phys. **9**, 248 (2013).

[9] C. J. Docherty, C.-T. Lin, H. J. Joyce, R. J. Nicholas, L. M. Herz, L.-J. Li, and M. B. Johnston, Nat. Commun. **3**, 1228 (2012).

[10] E. Yoo, T. Okata, T. Akita, M. Kohyama, J. Nakamura, and I. Honma, Nano Lett. **9**, 2255 (2009).

[11] M. Zhou, A. Zhang, Z. Dai, C. Zhang, and Y. P. Feng, J. Chem. Phys. **132**, 194704 (2010).

[12] K. Yamamoto, T. Imaoka, W.-J. Chun, O. Enoki, H. Katoh, M. Takenaga, and A. Sonoi, Nat. Chem. **1**, 397 (2009).

[13] Y. Li, Z. Zhou, G. Yu, W. Chen, and Z. Chen, J. Phys. Chem. C **114**, 6250 (2010).

[14] E. H. Song, Z. Wen, and Q. Jiang, J. Phys. Chem. C **115**, 3678 (2011).

[15] E. Ochoa-Fernández, D. Chen, Z. Yu, B. Tøtdal, M. Rønning, and A. Holmen, Surf. Sci. **554**, L107 (2004).

[16] Z.-J. Liu, Z. Xu, Z.-Y. Yuan, D. Lu, W. Chen, and W. Zhou, Catal. Lett. **72**, 203 (2001).

[17] H. Kim, W. Lee, and D. Yoo, Electrochim. Acta **52**, 2620 (2007).

[18] C. A. Bessel, K. Laubernds, N. M. Rodriguez, and R. T. K. Baker, J. Phys. Chem. B **105**, 1115 (2001).

[19] V. Selvaraj and M. Alagar, Electrochem. Commun. **9**, 1145 (2007).

[20] Z. Liu, X. Y. Ling, B. Guo, L. Hong, and J. Y. Lee, J. Power Sources **167**, 272 (2007).

[21] S. Kim and S.-J. Park, J. Solid State Electrochem. **11**, 821 (2007).

[22] J.-S. Zheng, X.-S. Zhang, P. Li, J. Zhu, X.-G. Zhou, and W.-K. Yuan, Electrochem. Commun. **9**, 895 (2007).

[23] R. Giordano, P. Serp, P. Kalck, Y. Kihn, J. Schreiber, C. Marhic, and J.-L. Duvail, Eur. J. Inorg. Chem. **2003**, 610 (2003).

[24] R. Xiao, D. Fritsch, M. D. Kuz'min, K. Koepernik, H. Eschrig, M. Richter, K. Vietze, and G. Seifert, Phys. Rev. Lett. **103**, 187201 (2009).

[25] S. Sahoo, A. Hucht, M. E. Gruner, G. Rollmann, P. Entel, A. Postnikov, J. Ferrer, L. Fernández-Seivane, M. Richter, D. Fritsch, and S. Sil, Phys. Rev. B **82**, 054418 (2010).

[26] T. O. Wehling, A. V. Balatsky, M. I. Katsnelson, A. I. Lichtenstein, and A. Rosch, Phys. Rev. B **81**, 115427 (2010).

[27] H. Johll, H. C. Kang, and E. S. Tok, Phys. Rev. B **79**, 245416 (2009).

[28] C. Cao, M. Wu, J. Jiang, and H.-P. Cheng, Phys. Rev. B **81**, 205424 (2010).

[29] K. T. Chan, J. B. Neaton, and M. L. Cohen, Phys. Rev. B **77**, 235430 (2008).

[30] H. Johll, J. Wu, S. W. Ong, H. C. Kang, and E. S. Tok, Phys. Rev. B **83**, 205408 (2011).

[31] D.-H. Lim, A. S. Negreira, and J. Wilcox, J. Phys. Chem. C **115**, 8961 (2011).

[32] R. C. Longo, J. Carrete, J. Ferrer, and L. J. Gallego, Phys. Rev. B **81**, 115418 (2010).

[33] J. Kotakoski, A. V. Krasheninnikov, U. Kaiser, and J. C. Meyer, Phys. Rev. Lett. **106**, 105505 (2011).

[34] L. Li, S. Reich, and J. Robertson, Phys. Rev. B **72**, 184109 (2005).

[35] J. M. Carlsson and M. Scheffler, Phys. Rev. Lett. **96**, 046806 (2006).

[36] X. Y. Cui, R. K. Zheng, Z. W. Liu, L. Li, B. Delley, C. Stampfl, and S. P. Ringer, Phys. Rev. B **84**, 125410 (2011).

[37] D. W. Boukhvalov and M. I. Katsnelson, Nano Lett. **8**, 4373 (2008).

[38] H. Wang, J. T. Robinson, G. Diankov, and H. Dai, J. Am. Chem. Soc. **132**, 3270 (2010).

[39] P. Kim, Nat. Mater. **9**, 792 (2010).

[40] A. Stone and D. Wales, Chem. Phys. Lett. **128**, 501 (1986).

[41] J. Kotakoski, J. C. Meyer, S. Kurasch, D. Santos-Cottin, U. Kaiser, and A. V. Krasheninnikov, Phys. Rev. B **83**, 245420 (2011).

[42] G.-D. Lee, C. Z. Wang, E. Yoon, N.-M. Hwang, D.-Y. Kim, and K. M. Ho, Phys. Rev. Lett. **95**, 205501 (2005).

[43] J. P. Perdew, K. Burke, and M. Ernzerhof, Phys. Rev. Lett. **77**, 3865 (1996).

[44] G. Kresse and J. Furthmüller, Comput. Mater. Sci. **6**, 15 (1996).

[45] G. Kresse and D. Joubert, Phys. Rev. B **59**, 1758 (1999).

[46] P. E. Blöchl, Phys. Rev. B **50**, 17953 (1994).

[47] O. Diéguez, M. M. G. Alemany, C. Rey, P. Ordejón, and L. J. Gallego, Phys. Rev. B **63**, 205407 (2001).

[48] H. Duan and Q. Zheng, Phys. Lett. A **280**, 333 (2001).

[49] G. Rollmann, M. E. Gruner, A. Hucht, R. Meyer, P. Entel, M. L. Tiago, and J. R. Chelikowsky, Phys. Rev. Lett. **99**, 083402 (2007).

[50] M. E. Gruner and P. Entel, J. Phys.: Condens. Matter **21**, 293201 (2009).

[51] G. Rollmann, P. Entel, and S. Sahoo, Comput. Mater. Sci. **35**, 275 (2006).

[52] S. Sahoo, "*Ab initio* study of free and deposited transition metal clusters," Ph.D. thesis, University of Duisburg-Essen, 2011.

[53] H. A. Jahn and E. Teller, Proc. R. Soc. London A **161**, 220 (1937).

[54] A. A. El-Barbary, R. H. Telling, C. P. Ewels, M. I. Heggie, and P. R. Briddon, Phys. Rev. B **68**, 144107 (2003).

[55] Y. Ma, P. O. Lehtinen, A. S. Foster, and R. M. Nieminen, New J. Phys. **6**, 68 (2004).

[56] B. R. K. Nanda, M. Sherafati, Z. S. Popovi, and S. Satpathy, New J. Phys. **14**, 083004 (2012).

[57] J. C. Meyer, C. Kisielowski, R. Erni, M. D. Rossell, M. F. Crommie, and A. Zettl, Nano Lett. **8**, 3582 (2008).

[58] V. V. Nelayev and A. I. Mironchik, Mater. Phys. Mech. **9**, 26 (2010).

[59] R. F. W. Bader, *Atoms in Molecules – A Quantum Theory* (Oxford University Press, 1994).

[60] W. Tang, E. Sanville, and G. Henkelman, J. Phys.: Condens. Matter **21**, 084204 (2009).

[61] W. Gao, J. E. Mueller, J. Anton, Q. Jiang, and T. Jacob, Angew. Chem. Int. Ed. **52**, 14237 (2013).

[62] Y. Okamoto, Chem. Phys. Lett. **420**, 382 (2006).